

CMS Physics Analysis Summary

Contact: cms-pag-conveners-exotica@cern.ch

2012/07/03

Search for Long-Lived Particles using Displaced Photons in pp Collisions at $\sqrt{s} = 7 \text{ TeV}$

The CMS Collaboration

Abstract

The results of a search for supersymmetry are presented using long-lived particles decaying into photons and invisible particles. Events were collected at a center-of-mass energy of 7 TeV in proton-proton collisions by the CMS detector at the LHC. The search is performed in the context of gauge-mediated symmetry breaking, where the lightest neutralino can have a non zero lifetime. The missing transverse energy and the time of impact of the photon on the surface of the electromagnetic calorimeter is used to search for an excess of events over the background expectation. After the final selection, using a data set of 4.86 fb^{-1} no significant excess is observed, and limits are set on the mass and proper decay length of the neutralino. Limits of $220 \text{ GeV}/c^2$ for its mass and 6000 mm on the proper decay length are set at 95 % CL.

1 Introduction

The standard model (SM) of particle physics has proven extremely successful, but despite its many successes still remains incomplete. New heavy particles with long lifetimes are predicted in many models of physics beyond the SM, such as hidden valley scenarios [1] or supersymmetry (SUSY) with gauge-mediated symmetry breaking (GMSB) [2]. These particles may be neutral and decay into photons and weakly interacting particles that escape detection.

Assuming R-parity is conserved, SUSY particles are produced in pairs and decay into SM particles (as well as other SUSY particles). Many versions of these models employ a similar phenomenology, so a benchmark scenario is chosen as the search model. This scenario is commonly described as ‘Snowmass Slope and Parameter Set 8’ (SPS8) [3]. In this scenario, the neutralino ($\tilde{\chi}_0^0$, the lightest mass eigenstate of the superpartners of the neutral gauge and Higgs bosons) is the next-to-lightest supersymmetric particle and decays almost exclusively into a photon (γ) and a weakly interacting gravitino (\tilde{G} , the superpartner of the graviton). The \tilde{G} is the lightest supersymmetric particle (LSP), and gives rise to a momentum imbalance in the transverse plane by leaving the detector without depositing energy. The dominant production mode of the $\tilde{\chi}_1^0$ is through a pair of gluinos via the strong interaction decaying via cascades. The $\tilde{\chi}_1^0$ is expected to be produced in association with high transverse momentum (p_T) jets. A Feynman diagram for this process can be seen in Figure 1. The search strategy for this study is therefore one high momentum photon produced in association with at least three high p_T jets. Although two photons are expected per event for GMSB, only a single photon is required to be identified. This is an attempt to remain open to displaced photon signals which do not have two photons per event. Searches for prompt photons from ATLAS [4] and D \emptyset [5] place the current most stringent lower limits on the mass of the $\tilde{\chi}_1^0$ in the SPS8 scenario at 175 GeV/c². Furthermore, searches for non-prompt photons from CDF [6] and CMS [7] place the most stringent lower limits on the lifetime of the $\tilde{\chi}_1^0$ at around 2 ns.

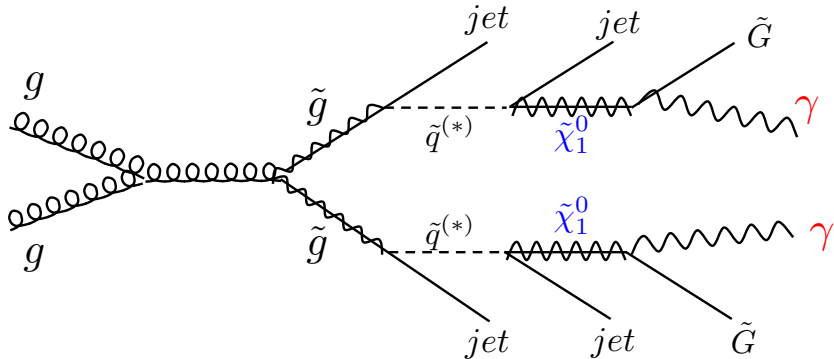


Figure 1: A Feynman diagram showing neutralino pair production and its subsequent decay in the $\tilde{\chi}_1^0 \rightarrow \tilde{G}\gamma$ process.

2 Detector and Data Samples

A detailed description of the CMS detector can be found elsewhere [8]. The detector’s central feature is a superconducting solenoid providing a 3.8 T axial magnetic field along the beam direction. Charged particle trajectories are measured by a silicon pixel and strip tracker system, covering $0 \leq \phi \leq 2\pi$ in azimuth and $|\eta| < 2.5$, where the pseudo-rapidity $|\eta|$ is defined as $\eta = \ln(\tan(\theta/2))$, and θ is the polar angle with respect to the counterclockwise beam direction.

A lead tungstate crystal electromagnetic calorimeter (ECAL) and a brass/scintillator hadron calorimeter (HCAL) surround the tracker volume. For the barrel part of the calorimeter ($|\eta| < 1.479$), the modules are arranged in projective towers. Muons are measured in gas detectors embedded in the steel return yoke of the magnet. The detector is nearly hermetic, allowing for reliable measurement of a transverse momentum imbalance. The data were recorded using the CMS two-level trigger system.

The data sample was collected in 2011 by the CMS detector at the LHC in pp collisions at a center-of-mass-energy of 7 TeV, corresponding to an integrated luminosity of $4.86 \pm 0.11 \text{ fb}^{-1}$. As mentioned previously, this analysis selects one high p_T isolated photon with at least three jets in the final state. For the initial period of 2011 data taking the primary trigger selected one isolated photon above a p_T of 75 GeV. For the middle part of data taking the primary trigger selected one isolated photon above a p_T of 90 GeV. Finally for the last part of data the primary trigger selected one isolated photon above a p_T of 90 GeV in the ECAL barrel with at least three jets above $p_T = 25$ GeV. All offline selection cuts are chosen to be tighter than the trigger selection. The Monte Carlo (MC) simulated events are generated using PYTHIA 6 [9] and MADGRAPH [10], and processed with a simulation of the CMS detector using the GEANT4 package [11]. Secondary τ decays are handled by TAUOLA [12]. For the GMSB signal, the generation follows the SPS8 proposal where the free parameters are the SUSY breaking scale (Λ) and the average $\tilde{\chi}_1^0$ proper decay length ($c\tau$). The free parameters are varied to cover an appropriate region of experimental phase space. We explore neutralinos in a mass range from 140 to 256 GeV/c² (corresponding to Λ values from 100 to 180 TeV) and with proper decay lengths ranging from 1 mm to 6000 mm (see Table 1).

Due to high luminosities produced by the LHC, there is a non-negligible probability that several collisions may occur in one single bunch-crossing. These are known as pile-up events and affect the resolution of the transverse momentum and the isolation variables. In order to account for their impact, the generated pile-up distribution in MC is re-weighted to mimic data taking conditions.

3 Analysis Technique

In this section the analysis technique is outlined. First, the physics object reconstruction is described, then event selection is briefly explained. Finally, the definition of the key discriminating variables related to the ECAL cluster shape and the time of impact of the photon on the surface of the ECAL are given.

3.1 Object Reconstruction

The photon reconstruction begins with the identification of energy deposits in the ECAL according to dedicated supercluster algorithms [13]. Jets are reconstructed from energy deposits in the calorimeters using the Particle Flow (PF) algorithm [14] with anti- k_T clustering [15] and a 0.5 distance parameter. Jets considered in this analysis are required to have $p_T \geq 35$ GeV and to be outside a cone of aperture $\Delta R = \sqrt{(\Delta\eta)^2 + (\Delta\phi)^2} = 0.5$ around the photon candidate. The missing transverse momentum vector is computed using the PF algorithm as the opposite of the transverse-momentum sum of all the particles in the event. Its length is referred to as the missing transverse energy (\cancel{E}_T).

The time of impact T_{raw} for the photon on the surface of the ECAL (ECAL time) is computed using the weighted time of impact of all the crystals within the supercluster associated to the signal photon. This is defined as

$$T_{raw} = \frac{\sum \frac{T_i}{\sigma_i^2}}{\sum \frac{1}{\sigma_i^2}}, \quad (1)$$

where T_i is the impact time measured by crystal i , and σ_i is the energy dependent uncertainty on its time measurement outlined in [16]. For T_{raw} , i runs along the indexes of all the crystals in the ECAL supercluster. In order to correct for detector mis-calibration and to reduce the error due to the uncertainty on the knowledge of the beam-spot position, the ECAL time measurement is calibrated using an event-by-event correction. This correction (T_{prompt}) is calculated as in Eqn. 1, where now, i runs over all the crystals in the event which do not belong to the clusters associated to the two most energetic photons. Since these crystals are not associated to the two most energetic photons, they are expected to come from prompt jets or low energy prompt photons. The new calibrated ECAL time (T_{calib}) is calculated with T_{prompt} and T_{raw} as

$$T_{calib} = T_{raw} - T_{prompt}. \quad (2)$$

An improvement of 0.1 ns is seen for the resolution for the ECAL timing using T_{calib} instead of T_{raw} . Furthermore, a difference in resolution of 0.4 ns for data, and 0.3 ns for MC is seen. In order to correct for this, the ECAL time distribution in MC is smeared as a function of photon energy to match what is observed in data. The distributions in data and MC for T_{raw} and T_{calib} are shown in Figure 2.

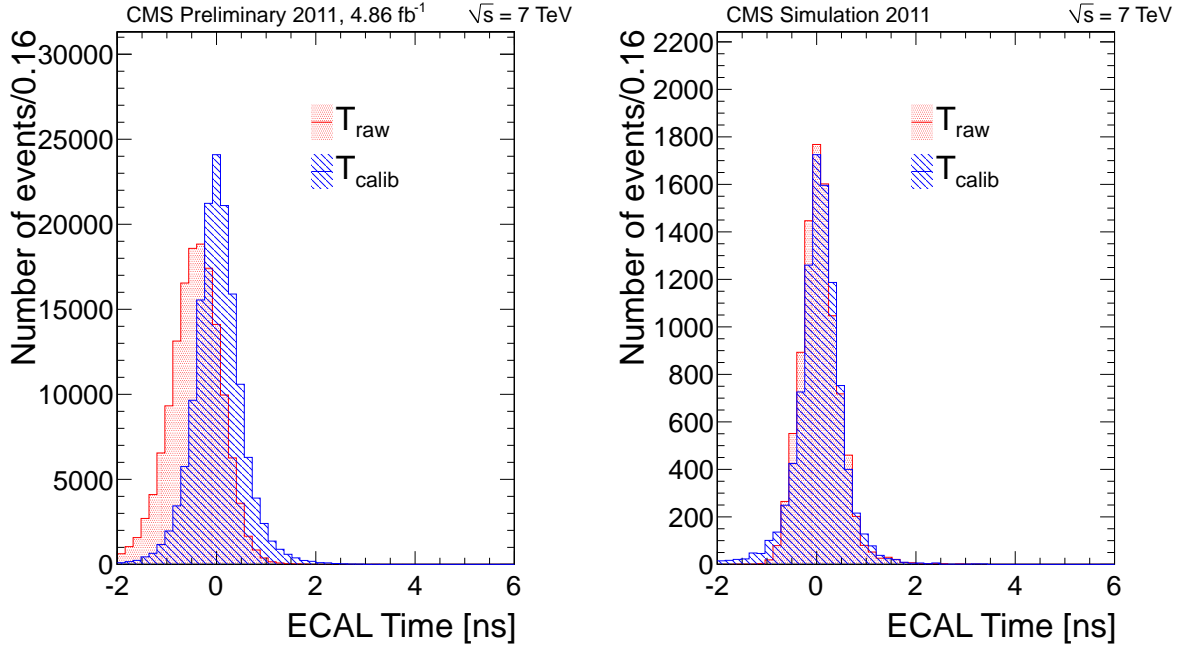


Figure 2: The ECAL time distribution for data (left) and MC (right) before and after calibrating.

3.2 Event Selection

A well reconstructed primary vertex is required with at least four associated tracks, whose position is less than 2 cm from the centre of the CMS detector in the direction transverse to the beam and 24 cm in the direction along the beam in each event. The photon candidate is required to have a p_T greater than 100 GeV and $|\eta|$ less than 1.4. A cone of size $\Delta R =$

$\sqrt{(\Delta\eta)^2 + (\Delta\phi)^2} = 0.4$ is constructed around the photon candidate, and the scalar sums of transverse energies of tracks and calorimeter deposits within this cone are determined, after excluding the contribution from the candidate itself. The photon candidate is required to be isolated in the HCAL, ECAL, and the tracker and absolute thresholds are placed as well as relative thresholds on the HCAL and ECAL isolation in order to prevent requirements which are tighter than the noise level of the calorimeters. In the HCAL and ECAL, the transverse energy deposited in the cone around the photon is required to be less than 5% of the photon E_T , and the absolute isolation required is less than 2.4 GeV. For the tracker isolation, the energy deposited in the cone around the photon is required to be less than 10% of the photon E_T . Electrons can be mis-reconstructed as photons, therefore any photon found within a ΔR cone of 0.25 of an electron is rejected.

3.3 Cluster Shape

One of the distinctive features of an off-pointing photon is the shape of the energy deposit it leaves in the ECAL. This is exploited by making a selection on the S_{Minor} variable which represents the minor axis of the photon ECAL cluster projection on the surface of the detector. Prompt photons are expected to have a roughly circular projected energy deposition on the ECAL surface, while delayed photons are expected to leave an elliptical energy deposition, as illustrated in Figure 3. In Figure 4 (right) the S_{Minor} distribution for data and MC is shown.

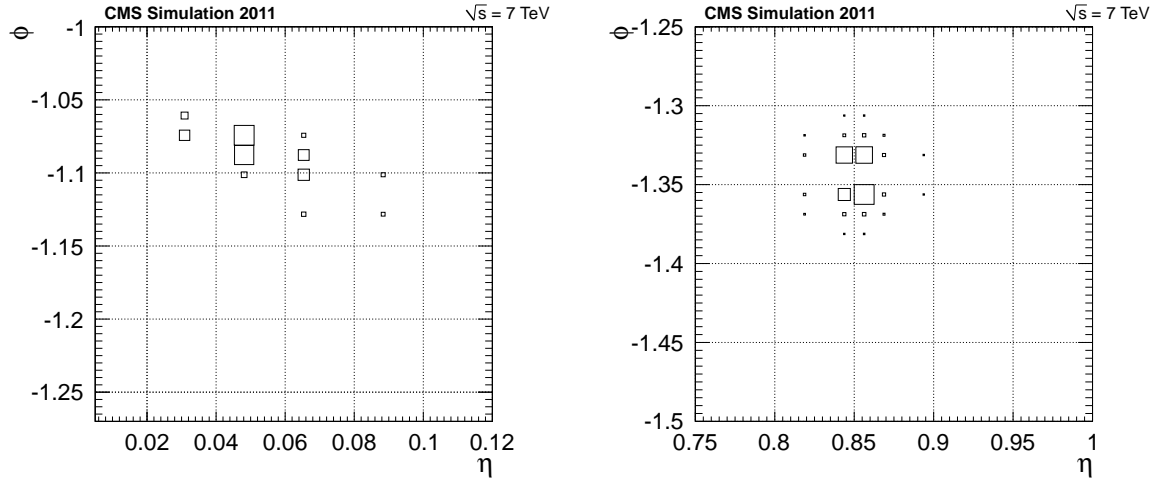


Figure 3: The energy distribution in the ECAL crystals for a displaced (left) and prompt (right) photon. Each bin represents an ECAL crystal and the size of the square is proportional to the energy in that crystal.

This cluster shape variable is computed using the geometrical properties of the energy deposit in the ECAL, as given by the following equation

$$S_{\text{Minor}} = \frac{S_{\phi\phi} + S_{\eta\eta} - \sqrt{(S_{\phi\phi} - S_{\eta\eta})^2 + 4S_{\phi\eta}^2}}{2} \quad (3)$$

where $S_{\mu\nu}$ are eigenvalues of the covariance matrix which describes the spatial distribution of the energy deposit in the ECAL. The ECAL cluster shape is required to be consistent with that expected from a photon, with $0.15 < S_{\text{Minor}} < 0.3$. The selection efficiencies after all cuts on the signal can be seen in Table 1.

Λ (TeV)	$M_{\tilde{\chi}_1^0}$ (GeV/c ²)	$c\tau = 1$ mm	$c\tau = 250$ mm	$c\tau = 2000$ mm	$c\tau = 6000$ mm
100	140	18.7 ± 0.3	18.4 ± 0.2	8.4 ± 0.2	3.3 ± 0.1
120	169	24.9 ± 0.4	24.6 ± 0.3	15.1 ± 0.4	6.6 ± 0.1
140	198	30.4 ± 0.3	31.3 ± 0.3	22.2 ± 0.4	11.4 ± 0.3
160	227	35.5 ± 0.3	36.1 ± 0.6	29.4 ± 0.4	17.0 ± 0.4
180	256	40.1 ± 0.7	38.0 ± 0.5	36.0 ± 0.5	22.2 ± 0.4

Table 1: The selection efficiencies in percent for MC signal.

4 Background Estimation

The main backgrounds in this analysis include multi-jet events which, due to finite resolution effects, give rise to “fake \cancel{E}_T ”. Alongside QCD multi-jet events there is also a contribution from γ +jet events. This is an important background due to the presence of a real isolated prompt photon in the final state and possible “fake \cancel{E}_T ” due to the jet not being fully reconstructed. However, γ +jet events are characterised by a lower jet multiplicity with respect to the signal, therefore a requirement on the minimum number of jets can reject a large fraction of this background. The contribution of these “fake \cancel{E}_T ” backgrounds are estimated to make up more than 99% of the total data sample and are estimated using data-driven control samples. Together with the processes giving rise to “fake \cancel{E}_T ”, a “real \cancel{E}_T ” contribution is expected. These are largely comprised of electroweak (EWK) decays and include $W \rightarrow l\nu$, where the lepton can be mis-reconstructed as a photon with the ν giving rise to real \cancel{E}_T in the event. For the same reasons, a contribution from $t\bar{t}$ decays is expected, where the top quark decays almost 100% of the time into a W boson and a b quark. The W boson then decays to leptons which can produce a $\gamma + \cancel{E}_T$ signature, with the \cancel{E}_T arising due to one or more neutrinos. We also expect a small contribution from Drell–Yan processes. These “real \cancel{E}_T ” events make up less than 1% of the total data sample but are still accounted for since they can play a role in the tails of the \cancel{E}_T distribution where signal is expected. Distributions of the photon p_T and S_{Minor} are illustrated in Figure 4 for data and MC events. The discrepancy between data and simulation is expected and is one of main motivations to use data-driven background estimates for multi-jet and gamma+jets events.

As mentioned previously, due to the difficulty in modelling the tails and predicting cross-sections of the multi-jet and γ +jet backgrounds, and accurately predicting kinematic distributions such as the number of jets data-driven techniques are used to estimate the main backgrounds (multi-jet and γ +jet). The multi-jet sample was obtained requiring events which pass a looser isolation selection, but fail the tight photon (with at least three jets) selection. The selection is as follows: in the HCAL and ECAL, the transverse energy deposited in the cone around the photon is required to be less than 50% of the photon E_T but greater than 5% (in order to keep the control sample statistically uncorrelated with the final sample). For the tracker, the energy deposited in the cone around the photon is required to be less than 45% of the photon E_T but greater than 10%. The γ +jet sample was obtained requiring one photon to pass the final selection, the most energetic jet (jet1) to be back to back with respect to the photon in the transverse plane, the ratio $p_T^{\text{jet1}}/p_T^\gamma$ to be between 0.6 and 1.4, and the ratio on the sub-leading jet ($p_T^{\text{jet2}}/p_T^\gamma$) to be less than 0.2. The EWK contamination for both the derived control samples is estimated to be less than 1%. Similarly, the signal contamination is less than 0.01%.

The remaining background contribution is estimated to be 0.6% of the total event sample. MC is used to estimate the contribution of these processes. Together with the backgrounds described above, events which do not originate from proton-proton collisions are also expected. These non-collision backgrounds include cosmic rays and beam-halo muons. In order to veto on these

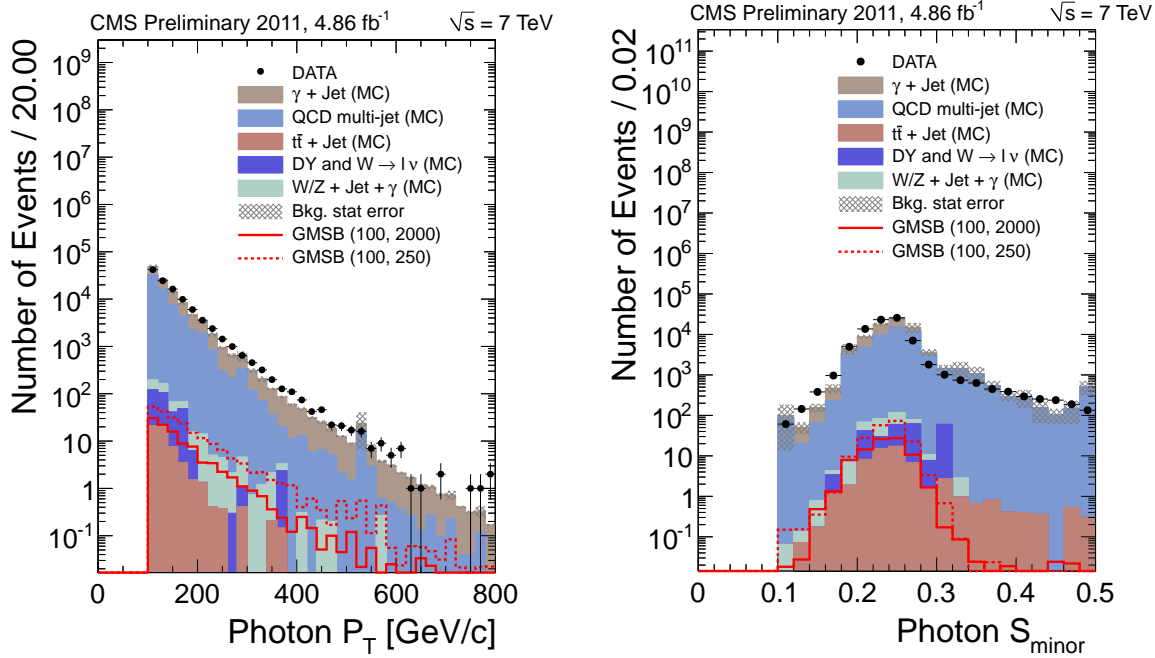


Figure 4: The distributions of the photon transverse momentum (left), and S_{Minor} (right) after all selection requirements data (points) and MC (solid) normalised to the luminosity of data. For this figure GMSB (100, 2000), corresponds to $\Lambda = 100 \text{ TeV}$, $c\tau = 2000 \text{ mm}$. Likewise, GMSB (100, 250) corresponds to $\Lambda = 100 \text{ TeV}$, $c\tau = 250 \text{ mm}$.

events the ECAL time is required to be greater than -0.2 ns. Furthermore, requiring the event to have a good primary vertex with at least three jets brings this non-collision contribution down to negligible levels.

In order to estimate the number of background and signal events in data, a maximum likelihood fit of signal + background is performed using the E_T and ECAL time distributions. The shape templates of the E_T and ECAL time are taken from the derived data control samples and MC. Shape templates for multi-jet and γ +jet, which are the main SM backgrounds are derived from data control samples. The relative normalisation of the multi-jet and γ +jet components is fixed to 67% and 33% respectively (calculated with MC). In order to improve the stability of the fit the MC background samples are normalised to the their cross section multiplied by the luminosity. These are thus fixed components in the fit. The 1D projections of the E_T and ECAL timing for all expected backgrounds and data can be seen in Figure 5. The number of events given from the fit are detailed in Table 2, where no excess beyond the expected SM contribution is seen.

5 Systematic Uncertainties

There are several sources of systematic uncertainty considered. The uncertainty on the luminosity is 2.2% [17]. The calorimeter response to particles is not linear and corrections are made to properly map the measured jet energy deposition. The uncertainty on this correction is referred to as the uncertainty on the jet energy scale and varies as a function of position and jet P_T . Similarly, the uncertainty on the photon energy scale in the barrel is estimated to be 1.0% and based on the final-state radiation measurement with Z bosons [18]. The uncertainties on the parton density functions (PDFs) are evaluated using the reweighting technique and Master

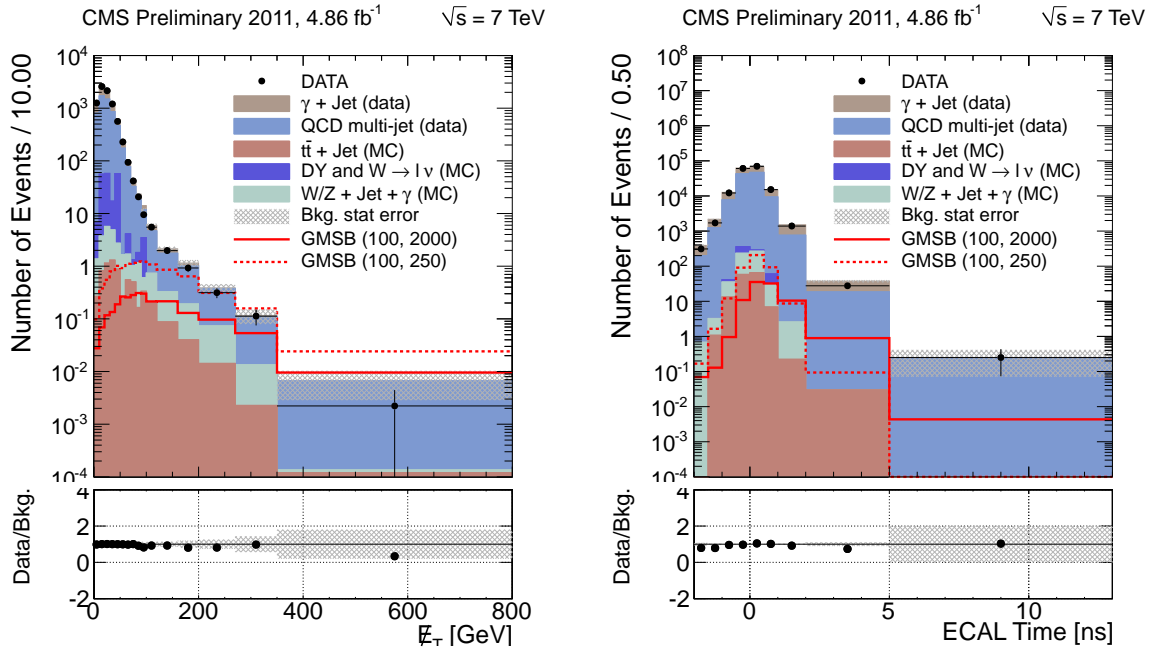


Figure 5: The 1D projections for the \mathcal{E}_T (left), and ECAL timing (right) after all selection requirements. The multi-jet and γ +jet backgrounds use shapes derived from data and are normalised using the fit. The rest of the backgrounds use shapes derived from MC and are normalised using the given cross sections. For this figure, GMSB (100, 2000) corresponds to $\Lambda = 100$ TeV, $c\tau = 2000$ mm. Likewise, GMSB (100, 250) corresponds to $\Lambda = 100$ TeV, $c\tau = 250$ mm.

	No. Events
GMSB (100, 250)	6 ± 8
GMSB (100, 2000)	4 ± 4
multi-jet and γ +jet	80916 ± 290
$t\bar{t}$ + jet (fixed)	73
$W \rightarrow e\nu$ + jet (fixed)	116
Drell-Yan + jet (fixed)	67
$W/Z + \text{jet} + \gamma$ (fixed)	215
Total background	81387
Data	81382

Table 2: The final number of events estimated for each component after all selection cuts and the fit to data. The relative composition of multi-jet and γ +jet have been normalised to 67% and 33% with respect to each other. The uncertainties listed correspond to the errors from the fit.

Equation on the CTEQ65 model set as described in Ref. [19]. The uncertainty on the \mathcal{E}_T resolution uses the conservative estimate of 10%. A conservative estimate of 0.1 ns is made on the uncertainty due to the ECAL time. This was derived from a performance study of γ +jet events. For the uncertainty on the background estimation both the uncertainty due to the normalisation and in the shape are considered. The uncertainty on the normalisation is taken from the error on the fit. The uncertainty on the shape is assessed by varying the background shape bin-by-bin according to the Poisson uncertainty due to statistics. The uncertainty on the derived shape of the data-driven backgrounds is assessed by re-weighting the \mathcal{E}_T and ECAL time according to differences seen in the shapes of the MC control sample and default selection. The

re-weighting is performed across the entire spectrum of E_T and ECAL timing in order to derive a conservative estimate. The uncertainty on the fraction used to fix the multi-jet and γ +jet ratio in the fit is calculated by finding the difference in the total event yield between γ +jet MC and data control sample. The uncertainties due to PYTHIA cross-sections are expected to manifest themselves as this difference. A summary of all the systematic uncertainties are listed in Table 3.

Source	Uncertainty (%)
Signal efficiency:	
Photon energy scale	< 3.0
Jet energy scale	< 0.05
Jet energy resolution	< 1.9
PDF uncertainties	< 1.7
Signal shape:	
E_T resolution	< 1.5
ECAL time uncertainty	< 5.0
Background:	
Shape	< 10.5
Normalisation	< 0.3
Multi-jet/ γ + jet fraction	< 0.5

Table 3: Summary of the systematic uncertainties. The uncertainties are evaluated individually for each signal point, but for brevity only the maximum value associated to each source is quoted in this table.

6 Results

Since the estimated number signal events is compatible with zero, upper-limits on the GMSB cross section are set at 95% confidence level (CL). The computation for the GMSB cross section limit is made using the CLs [20, 21] method, and the asymptotic approximation for the test statistic as described in [22]. The uncertainties for the luminosity and signal acceptance are accounted for using log-normal multiplicative corrections. The shapes of 2D distributions are inputted for the E_T and ECAL timing for both signal and background, along with the normalisation of the expected background given by the fit. The main sources of uncertainty are on the shape of the signal and background templates. Figure 6 shows the observed and expected 95% CL upper limits on the cross section for GMSB production in terms of $\tilde{\chi}_1^0$ mass (left), and proper decay length (right). The limits are derived under the assumption that the branching fraction for the neutralino decay $BR(\tilde{\chi}_1^0 \rightarrow \gamma \tilde{G}) = 100\%$. The upper limit for the neutralino mass and proper decay length is given by the value at which the observed upper limit curve for the cross section crosses the theoretical curve. In the plot on the left of Figure 6 this happens for the 95% CL observed limits for a $\tilde{\chi}_1^0$ mass of 220 GeV/c². In the plot on the right of Figure 6 the limit on the proper decay length $c\tau$ is shown to be 6000 mm. An exclusion plot in the mass and proper decay length plane of the $\tilde{\chi}_1^0$ is shown in Figure 7. These results significantly improve our knowledge of the $\tilde{\chi}_1^0$ in the SPS8 model of GMSB supersymmetry beyond those of the D \emptyset , CDF, and ATLAS collaborations.

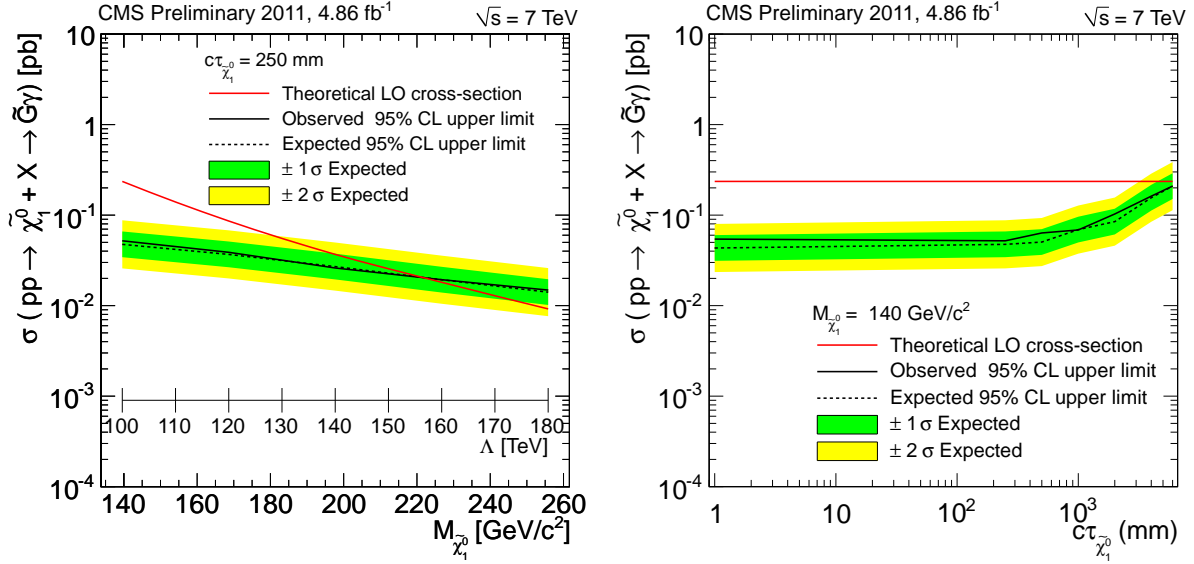


Figure 6: The observed 95% CL cross section upper limits as a function of the $\tilde{\chi}_1^0$ mass for $c\tau = 250$ mm (left), and the $\tilde{\chi}_1^0$ proper decay length for $M_{\tilde{\chi}_1^0} = 140$ GeV/c^2 (right) for SPS8.

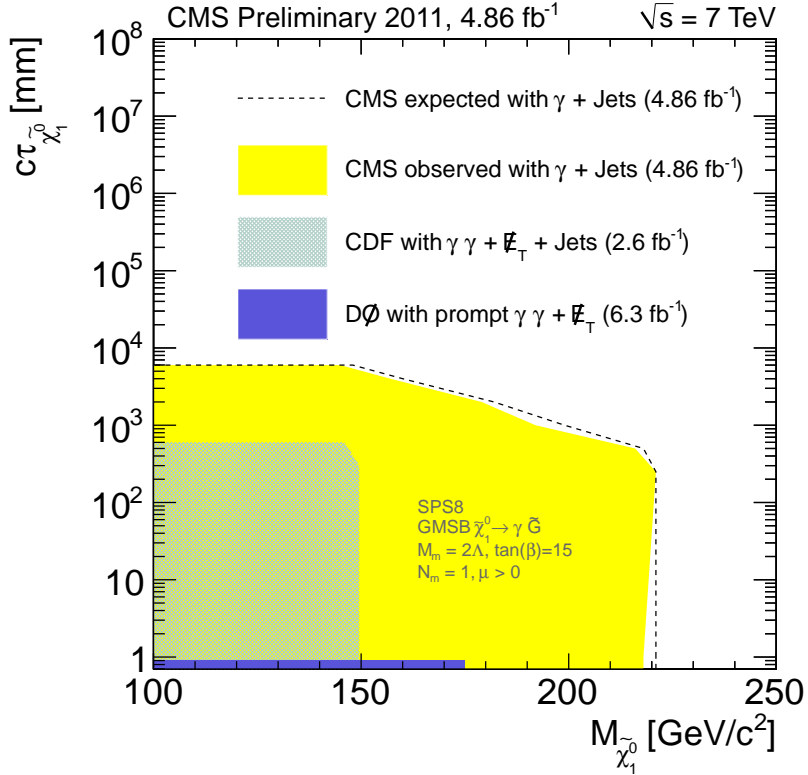


Figure 7: The observed exclusion region for the mass and proper decay length of the $\tilde{\chi}_1^0$.

7 Summary

The CMS experiment has performed a search for long-lived particles produced in association with jets using $4.86 \pm 0.11 \text{ fb}^{-1}$ of proton-proton collision data at the centre-of-mass energy of 7 TeV. The missing transverse energy and timing information from the ECAL is used to search for

an excess of events over the expected SM background prediction. After all selection requirements, the data is found to be in agreement with the expected contributions from standard model processes. Upper limits at 95% C.L. are then set on the GMSB cross section in SPS8. From the upper limits a mass below $220 \text{ GeV}/c^2$ and below $c\tau 6000 \text{ mm}$ can be excluded for the $\tilde{\chi}_1^0$.

References

- [1] M. J. Strassler and K. M. Zurek, “Echoes of a hidden valley at hadron colliders”, *Phys.Lett.* **B651** (2007) 374–379, doi:10.1016/j.physletb.2007.06.055, arXiv:hep-ph/0604261.
- [2] G. F. Giudice and R. Rattazzi, “Theories with gauge-mediated supersymmetry breaking”, *Phys. Rept.* **322** (1999) 419–499, doi:10.1016/S0370-1573(99)00042-3, arXiv:hep-ph/9801271.
- [3] B. C. Allanach et al., “The Snowmass points and slopes: Benchmarks for SUSY searches”, *Eur. Phys. J.* **C25** (2002) 113–123, doi:10.1007/s10052-002-0949-3, arXiv:hep-ph/0202233.
- [4] ATLAS Collaboration Collaboration, “Search for Diphoton Events with Large Missing Transverse Momentum in 1 fb^{-1} of 7 TeV Proton-Proton Collision Data with the ATLAS Detector”, *Phys.Lett.* **B710** (2012) 519–537, arXiv:1111.4116.
- [5] D0 Collaboration Collaboration, “Search for diphoton events with large missing transverse energy in 6.3 fb^{-1} of $\text{p}\bar{\text{p}}$ collisions at $\sqrt{s} = 1.96 \text{ TeV}$ ”, *Phys.Rev.Lett.* **105** (2010) 221802, doi:10.1103/PhysRevLett.105.221802, arXiv:1008.2133.
- [6] CDF Collaboration, “Search for Supersymmetry with Gauge-Mediated Breaking in Diphoton Events with Missing Transverse Energy at CDF II”, *Phys. Rev. Lett.* **104** (2010) 011801, doi:10.1103/PhysRevLett.104.011801, arXiv:0910.3606.
- [7] CMS Collaboration, “Search for new physics with long-lived particles decaying to photons and missing energy”, *EXO-11-067* (2011).
- [8] CMS Collaboration Collaboration, “The CMS experiment at the CERN LHC”, *JINST* **3** (2008) S08004, doi:10.1088/1748-0221/3/08/S08004.
- [9] T. Sjöstrand, S. Mrenna, and P. Z. Skands, “PYTHIA 6.4 Physics and Manual”, *JHEP* **05** (2006) 026, doi:10.1088/1126-6708/2006/05/026, arXiv:hep-ph/0603175.
- [10] J. Alwall, M. Herquet, F. Maltoni et al., “MadGraph 5 : Going Beyond”, *JHEP* **1106** (2011) 128, doi:10.1007/JHEP06(2011)128, arXiv:1106.0522.
- [11] GEANT4 Collaboration, “GEANT4: A simulation toolkit”, *Nucl. Instrum. Meth.* **A506** (2003) 250–303, doi:10.1016/S0168-9002(03)01368-8.
- [12] Z. Was, “TAUOLA the library for tau lepton decay, and KKMC/KORALB/KORALZ/... status report”, *Nucl. Phys. Proc. Suppl.* **98** (2001) 96–102, doi:10.1016/S0920-5632(01)01200-2, arXiv:hep-ph/0011305.
- [13] CMS Collaboration, “Isolated Photon Reconstruction and Identification at \sqrt{s} ”, *CMS PAS EGM-10-006* (2011).

- [14] CMS Collaboration, “Commissioning of the Particle-Flow Reconstruction in Minimum-Bias and Jet Events from pp Collisions at 7 TeV”, *CMS PAS PFT-10-002* (2010).
- [15] CMS Collaboration, “The anti- kt jet clustering algorithm”, *JHEP* **0804** (2008) 6374, doi:10.1088/1126-6708/2008/04/063.
- [16] CMS Collaboration, “Time Reconstruction and Performance of the CMS Electromagnetic Calorimeter”, *JINST* **5** (2010) T03011, doi:10.1088/1748-0221/5/03/T03011, arXiv:0911.4044.
- [17] CMS Collaboration Collaboration, “Absolute Calibration of Luminosity Measurement at CMS: Winter 2012 Update”, *CMS-PAS-SMP-12-008* (2012).
- [18] CMS Collaboration Collaboration, “Measurement of $W\gamma$ and $Z\gamma$ production in pp collisions at”, *Physics Letters B* **701** (2011), no. 5, 535 – 555, doi:10.1016/j.physletb.2011.06.034.
- [19] A. Martin, W. Stirling, R. Thorne et al., “Parton distributions for the LHC”, *Eur.Phys.J.* **C63** (2009) 189–285, doi:10.1140/epjc/s10052-009-1072-5, arXiv:0901.0002.
- [20] T. Junk, “Condence Level Computation for Combining Searches with Small Statistics”, *Nucl. Instrum. Meth.* **A** (1999) 434–435.
- [21] A. L. Read, “Presentation of search results: The CL(s) technique”, *J.Phys.G* **G28** (2002) 2693–2704, doi:10.1088/0954-3899/28/10/313.
- [22] G. Cowan, K. Cranmer, E. Gross et al., “Asymptotic formulae for likelihood-based tests of new physics”, *Eur.Phys.J.* **C71** (2011) 1554, doi:10.1140/epjc/s10052-011-1554-0, arXiv:1007.1727.